Received: 29 January 2020 | Revised: 8 July 2020 | Accepted: 16 July 2020

DOI: 10.1002/jnr.24707

RESEARCH ARTICLE

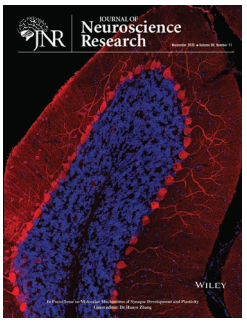

Quantification of aromatase binding in the female human brain using [^{11}C]cetrozole positron emission tomography

My Jonasson[1,2] | Patrik Nordeman[3,4] | Jonas Eriksson[3,4] | Helena Wilking[4] | Johan Wikström[1] | Kayo Takahashi[5] | Takashi Niwa[5] | Takamitsu Hosoya[5,6] | Yasuyoshi Watanabe[5] | Gunnar Antoni[3,4] | Inger Sundström Poromaa[7] | Mark Lubberink[1,2] | Erika Comasco[8]

[1]Department of Surgical Sciences, Uppsala University, Uppsala, Sweden

[2]Department of Medical Physics, Uppsala University Hospital, Uppsala, Sweden

[3]Department of Medicinal Chemistry, Uppsala University, Uppsala, Sweden

[4]PET centre, Uppsala University Hospital, Uppsala, Sweden

[5]RIKEN Center for Biosystems Dynamics Research, Kobe, Japan

[6]Institute of Biomaterials and Bioengineering, Tokyo Medical and Dental University, Tokyo, Japan

[7]Department of Women's and Children's Health, Uppsala University, Uppsala, Sweden

[8]Department of Neuroscience, Science for Life Laboratory, Uppsala University, Uppsala, Sweden

Correspondence
My Jonasson, Department of Surgical Sciences, Uppsala University, 751 85 Uppsala, Sweden.
Email: my.jonasson@radiol.uu.se

Erika Comasco, Department of Neuroscience, Science for Life Laboratory, Uppsala University, 75 124 Uppsala, Sweden
Email: Erika.comasco@neuro.uu.se

Funding information
ALF; Swedish Research Council, Grant/Award Number: VR: 2015-00495; EU FP7-People-Cofund, Grant/Award Number: INCA 600398; SciLifeLab

Abstract

Aromatase, the enzyme that in the brain converts testosterone and androstenedione to estradiol and estrone, respectively, is a putative key factor in psychoneuroendocrinology. *In vivo* assessment of aromatase was performed to evaluate tracer kinetic models and optimal scan duration, for quantitative analysis of the aromatase positron emission tomography (PET) ligand [^{11}C]cetrozole. Anatomical magnetic resonance and 90-min dynamic [^{11}C]cetrozole PET-CT scans were performed on healthy women. Volume of interest (VOI)-based analyses with a plasma-input function were performed using the single-tissue and two-tissue (2TCM) reversible compartment models and plasma-input Logan analysis. Additionally, the simplified reference tissue model (SRTM), Logan reference tissue model (LRTM), and standardized uptake volume ratio model, with cerebellum as reference region, were evaluated. Parametric images were generated and regionally averaged voxel values were compared with VOI-based analyses of the reference tissue models. The optimal reference model was used for evaluation of a decreased scan duration. Differences between the plasma-input- and reference tissue-based methods and comparisons between scan durations were assessed by linear regression. The [^{11}C]cetrozole time–activity curves were best described by the 2TCM. SRTM nondisplaceable binding potential (BP_{ND}), with cerebellum as reference region, can be used to estimate [^{11}C]cetrozole binding and generated robust and quantitatively accurate results for a reduced scan duration of 60 min. Receptor parametric mapping, a basis function implementation of SRTM, as well as LRTM, produced quantitatively accurate parametric images, showing BP_{ND} at the voxel level. As PET tracer, [^{11}C]cetrozole can be employed for relatively short brain scans to measure aromatase binding using a reference tissue-based approach.

Edited by Constanza Cortes. Associate Editor: Eric M. Prager. Reviewed by Andrea Varrone.

Mark Lubberink and Erika Comasco shared authorship.

KEYWORDS
aromatase, brain, cetrozole, kinetic modeling, positron emission tomography, women

1 | INTRODUCTION

Aromatase is the enzyme that converts androgens into estrogens (Thomas & Potter, 2013). Besides its role in reproduction, and its presence in the ovary, testis, and adipose fat tissue, aromatase is present in the brain and involved in neuronal survival, emotional behavior and cognition (Brocca & Garcia-Segura, 2019). Moreover, altered levels of aromatase have been found in different brain regions of patients with Alzheimer's disease and depression (Ishunina et al., 2005; Wu et al., 2017). However, the association between aromatase and brain functions is not fully understood.

Fine mapping and quantification of regional brain expression of aromatase *in vivo* are important to better understand physiological and pathological conditions. To assess aromatase *in vivo*, positron emission tomography (PET) combined with carbon-11 labeled reversible aromatase inhibitors has been employed, using tracers like [^{11}C]vorozole (Biegon et al., 2010, 2015) and, more recently, [^{11}C]cetrozole (Takahashi et al., 2018). Further quantification of aromatase binding can be performed by applying suitable mathematical models on the data both on the regional level, in specific volumes of interests (VOIs), and on a voxel level, to produce parametric images. In humans, the highest binding to aromatase has been found in the thalamus and hypothalamus, followed by the medulla, amygdala, nucleus accumbens, caudate nucleus, putamen, hippocampus, and cortex (Biegon, 2015; Biegon et al., 2010, 2015; Takahashi et al., 2018), thus in brain regions of relevance for reproductive as well as mental functions. On the other hand, the cerebellum has been selected as reference region because of low aromatase expression (Biegon, 2015; Biegon et al., 2010, 2015; Takahashi et al., 2018). This is in line with postmortem analyses demonstrating mRNA levels being highest in the hypothalamus and thalamus, intermediate in the amygdala and hippocampus followed by the frontal cortex, and lowest in the cerebellum (Sasano, Takashashi, Satoh, Nagura, & Harada, 1998).

The novel aromatase radioligand [^{11}C]cetrozole has been shown to bind specifically to aromatase, with higher signal-to-noise ratio than [^{11}C]vorozole in nonhuman primates and without accumulation of radiolabeled metabolites in the brain of rats (Takahashi et al., 2014). In humans, [^{11}C]cetrozole binding in men was found to be higher in the left hypothalamus than in women (Takahashi et al., 2018); additionally, [^{11}C]cetrozole binding in the left amygdala correlated positively with aggressiveness in the women. In previous studies with [^{11}C]cetrozole, both in humans and nonhuman primates, aromatase was quantified using plasma-input function as well as reference region approaches (Takahashi et al., 2014, 2018), but no extensive validation of tracer kinetic models or methods for generating parametric images has been performed for this tracer. Thus, the aims of the present study were to (a) evaluate tracer kinetic models (Gunn, Gunn, & Cunningham, 2001) for quantitative analysis of [^{11}C]cetrozole in humans, based on plasma- and reference tissue input data, (b) to evaluate methods for producing parametric images of aromatase binding, and (c) to investigate the effect of scan duration on the above outcome parameters. The identification of optimal modeling to quantify [^{11}C]cetrozole uptake and scanning protocol are presented.

Significance

Estrogens synthesis is regulated by aromatase, an enzyme whose level can be assessed in the brain by use of a biochemical imaging technique. Optimal steps for aromatase analysis were identified by employing this neurotechnique on healthy women using the selective aromatase inhibitor cetrozole. As the association between aromatase and brain functions is not fully understood, quantitative studies in living humans are of importance to gain knowledge on the relation between aromatase expression and physiological and pathological processes.

2 | MATERIALS AND METHODS

2.1 | Participants

As part of the "Brain Sex Hormones" (BSH) project, 13 healthy women were recruited by public announcements for participation in the present study. The study was conducted at the Department of Women's and Children's Health, Uppsala University and PET Centre, Uppsala University Hospital, between 2016 and 2018. We included Swedish-speaking women with heterosexual orientation and Caucasian origin, aged 20–35 years, with regular menstrual cycles (25–34 days), right-handed, BMI < 30 kg/m^2, blood pressure <140/90 mmHg, and no self-reported health issues. Women were excluded if they had ongoing or previous mental health conditions, ongoing or recent (<6 months) pregnancy, abortion or delivery, ongoing hormonal treatment (including hormonal contraceptives), ongoing or previous nicotine use, or if they were treated with psychotropic medication. Mental health was assessed by means of the Mini International Neuropsychiatric Interview (Sheehan et al., 1998). All participants received monetary compensation. The study procedure was in accordance with ethical standards for human experimentation (Helsinki declaration) and was approved by the Regional Ethical Review Board of Uppsala (2014/393), and the Medical Radiation Ethics Committee of Uppsala University Hospital.

2.2 | Synthesis of [^{11}C]cetrozole

[^{11}C]Cetrozole (4-((4-[^{11}C]methylbenzyl)(4H-1,2,4-triazol-4-yl)amino) benzonitrile) ready for injection was produced according to good manufacturing practice at Uppsala University Hospital using fully automated synthesis equipment (TPS, built in-house). The synthesis was based on the method described by Takahashi et al. (2014) but with reduced reagent loads and prefiltration of the reagent mixture. In short, the boronic ester containing precursor MD-298 (4-((4-(4,4,5,5-tetramethyl-1,3,2-dioxaborolan-2-yl)benzyl)(4H-1,2,4-triazol-4-yl)amino) benzonitrile) (1.0 mg), $Pd_2(dba)_3$ (0.8 mg), P(*o*-Tol)$_3$ (1.0 mg), and K_2CO_3 (1.0 mg) were added to a filter cartridge Mini-uniprep™ PP filter (GE) and dissolved in DMF (300 μl). The solution was then filtered and transferred to a conical glass reaction vial equipped with septum. Cyclotron-produced [^{11}C]carbon dioxide was converted to [^{11}C]methyl iodide by the "wet method" and transferred to the reagent solution in a stream of nitrogen gas. The resulting mixture was heated at 65°C for 2 min, diluted with an acetonitrile-water mixture (40/60, 2 ml), and [^{11}C]cetrozole was then purified and isolated by semi-preparative HPLC (ammoniumcarbonate 8.1 mM:acetonitrile; Chromosil Cholester 5 μm, 10 × 250 mm, Nacalai Tesque). The HPLC eluent was removed by vortex evaporation and the product was reformulated in ethanol (0.5 ml), Kleptose HPB (hydroxypropyl-β-cyclodextrin in sodium chloride 9 mg/ml, 300 mg/ml, 0.8 ml), and phosphate buffer pH 7.4 (0.1 M, 5 ml) and filtered through a 0.22-μm sterile filter (Millex-GV, Millipore) into a sterile glass vial. Radiochemical purity, identity, and concentration of the labeled product were assessed by analytical HPLC (ammoniumcarbonate 8.1 mM:acetonitrile; Gemini NX C18, Phenomenex, 4.6 × 100 mm) equipped with radio and UV detectors and isotopically unmodified cetrozole was used as reference. The palladium concentration in the product solution was quantified by ICP-AES.

2.3 | Data acquisition

Participants were instructed to abstain from caffeine and alcohol intake within the previous 12 hr, as well as food intake 3 hr prior to the session. Pregnancy tests were checked negative. The PET scans were acquired using either a Discovery ST (10 scans), Discovery IQ (two scans), or Discovery MI (18 scans) PET/CT scanner (GE Healthcare, Milwaukee, WI, USA), at baseline and after two challenges in random order (that is three scans for each participant, given the fact that no effect of challenge was observed on kinetic modeling, as reported in the results section). After a low-dose computed tomography (CT), performed for attenuation correction, 4.0 ± 0.7 MBq/kg [^{11}C]cetrozole was administered as a bolus, simultaneously with the start of a 90-min dynamic PET scan of 26 frames of increasing length (6 × 10, 3 × 20, 2 × 30, 3 × 60, 2 × 120, 4 × 300, 6 × 600 s). Reconstruction settings were chosen to yield similar spatial resolution across the three scanner models used: Ordered Subsets Expectation Maximization with two iterations and 21 subsets and a 4-mm postprocessing filter for the Discovery ST, four iterations and 12 subsets and a 4-mm postprocessing filter for the Discovery IQ, and three iterations and 34 subsets and a 5-mm postprocessing filter for the Discovery MI, with a resulting spatial resolution of about 6 mm. All appropriate corrections resulting in quantitative images were performed on the PET data. During eight scans, online blood sampling (Veenstra Instruments, Joure, The Netherlands) from a radial artery cannula was performed during the first 10 min of the scan (3 ml/min). Discrete blood samples (5 ml) were also taken at 5, 10, 15, 20, 30, 40, 50, 60, 70, 80, and 90-min postinjection for measurements of whole blood and plasma radioactivity and for metabolite analysis. In addition, all subjects underwent a T1-weighted magnetic resonance image (MRI) scan on a 3T Achieva scanner (Philips Healthcare, Best, The Netherlands) at the Department of Radiology for anatomical information and for VOI definition.

2.4 | Radiometabolite analysis

Blood was collected in heparin tubes and plasma was separated by centrifugation. The percentage of intact [^{11}C]cetrozole in plasma was determined by high-performance liquid chromatography (HPLC). Plasma was precipitated using acetonitrile, and the supernatant was filtered and spiked with unlabeled cetrozole for identification. A 1.8-ml sample was injected onto a semi-preparative HPLC column (Genesis C18, 7 μm, 250 × 10 mm, Phenomenex) equipped with a guard column (C18 SecurityGuard, 10 × 10 mm, Phenomenex). The column was eluted at a flow rate of 6 ml/min with acetonitrile −50 mM and ammonium carbonate 8.1 mM (55:45, v/v). The outlet from the detector was connected to a switching valve on the arm of the liquid handler to enable automatic fraction collection. Three fractions were collected, where the third contained the parent compound. The radioactivity in each fraction was measured by a well-type scintillation counter. The continuous arterial sampling data were calibrated relative to the discrete samples using the overlapping samples at 5 and 10 min postinjection. The arterial input function was obtained by multiplying the measured whole blood data by a single exponential fit to plasma/whole blood ratios, and a sigmoid fit to the measured fraction of intact [^{11}C]cetrozole in plasma.

2.5 | Image analysis

The dynamic [^{11}C]cetrozole PET data were corrected for interframe subject movement using VOIager software (GE Healthcare, Uppsala, Sweden). The MRI scans were co-registered to the sum of the first 5 min of the PET scan based on a 6-parameter rigid transformation using SPM8 (Wellcome Trust Center for Neuroimaging, University College London, UK). The MR images were segmented into gray matter, white matter, and CSF using SPM8. Six VOIs were included in the data analysis: thalamus, amygdala, hypothalamus, putamen, raphe nuclei, and cerebellum, averaged over the left and right sides. All VOIs, except amygdala, were defined using an automated probabilistic VOI template as implemented in the software PVElab (Svarer et al., 2005). The amygdala VOIs were defined using a 70% isocontour VOI, drawn on precalculated parametric images of the [^{11}C]cetrozole binding (see

Figure 5). The acquired VOIs were projected over all frames of the dynamic PET data to obtain time–activity curves (TACs).

2.6 | Tracer kinetic analysis

Single-tissue (1TCM) and two-tissue (2TCM) reversible plasma-input compartment models were applied to all TACs, using nonlinear regression with blood volume as an additional fit parameter. Nondisplaceable binding potential (BP_{ND}) was calculated both directly (for 2TCM) as well as indirectly as the ratio of the volumes of distribution (V_T) in the target and reference regions minus one (DVR-1), with cerebellum gray matter as reference region. The optimal plasma-input model was determined using the Akaike information criterion (AIC; Akaike, 1974). In addition, plasma-input Logan analyses (Logan et al., 1990) were performed, estimating the binding as DVR-1.

Reference tissue models were also applied using cerebellum gray matter as reference region (Takahashi et al., 2014). BP_{ND} was calculated using the simplified reference tissue model (SRTM) (Lammertsma & Hume, 1996) and DVR-1 was calculated using Logan reference tissue model (LRTM) (Logan et al., 1996). LRTM analysis was done both with and without the efflux constant, k_2, in the model, with this constant based on 1TCM k_2 values in cerebellum (Logan et al., 1996). BP_{ND} was also estimated using the standardized uptake value ratio (SUVR) minus one (SUVR-1), calculated as the ratio of the radioactivity concentration in each VOI relative to the reference region, on an interval of 80–90 min ($SUVR_{80-90}$–1). The reference tissue methods were validated by comparison of BP_{ND} or DVR-1 values with DVR-1 values based on the optimal plasma-input compartment model and plasma-input Logan analyses by calculating the orthogonal regression the square of the Pearson's correlation coefficient (R^2) and the bias.

2.7 | Parametric images

Voxel-level analysis was performed to generate parametric images showing the [^{11}C]cetrozole binding for each voxel. The basis function implementation of SRTM (RPM) (Gunn, Lammertsma, Hume, & Cunningham, 1997) and the two-parameter version of SRTM (RPM2) (Wu & Carson, 2002) were used, with a set of 50 basis functions with clearance rate values ranging from 0.01 to 2.00, to calculate BP_{ND} for each voxel. The number of estimated parameters was reduced to two for RPM2 by assuming a constant efflux rate constant from the reference tissue, k_2', in the whole brain. This value was determined by taking the median k_2' value from the previous RPM analysis in all voxels with a BP_{ND} value > 0. In addition, LRTM DVR-1 was also estimated for each voxel. Quantitative evaluation of the parametric methods was performed by projecting the set of VOIs used for analysis onto the parametric images to retrieve regionally averaged BP_{ND} and DVR-1 values. The values from the parametric images were compared to the optimal VOI-based reference method using orthogonal regression and correlation analysis. Plasma-input and reference tissue modeling, as well as generating the parametric images, were performed using in-house developed software in Matlab (The Mathworks, Natick, USA).

2.8 | Scan duration

In addition to the 90-min scan data, shortened data sets of the initial 40 min (21 frames) and 60 min (23 frames) were extracted from the dynamic scans to evaluate the minimum scan duration needed for quantification of [^{11}C]cetrozole. BP_{ND} was calculated using SRTM for both the 40- and 60-min data sets. DVR-1 was calculated using LRTM, at time intervals of 20–40 and 30–60 min, and SUVR-1 were estimated at 30–40 and 50–60 min. Absolute bias was calculated between BP_{ND}, DVR-1, or SUVR-1 of the shorter scan durations and the full 90-min scan.

2.9 | Simulations

To assess the robustness of the outcome measures, three sets of 100 noisy TACs were simulated using the two-tissue compartment model, using typical rate constant values for high, medium, and low binding, representing thalamus, amygdala, and raphe as well as cerebellum as reference tissue. Noise was added with levels similar to those seen in the clinical data, and the simulated TACs were fitted with the compartment models described above. Accuracy and precision of V_T, DVR-1, BP_{ND} were calculated as the bias and coefficient of variation (COV).

2.10 | Statistics

Analyses for symmetrical regions were based on averages of left and right. Analysis of tracer kinetic models and parametric images was performed by the use of orthogonal linear regression and Pearson correlation tests in GraphPad Prism (GraphPad Software, San Diego, Ca, USA). In addition, a multilinear regression was done to assess the effect of each challenge on the correlation between plasma-input and reference tissue models.

3 | RESULTS

3.1 | Subjects

Three subjects were excluded from the analysis due to incomplete PET data and subsequent dropout of the study, thus the final data set comprised of 30 scans, three for each woman. The 10 participants included in the analyses were healthy, naturally cycling women (mean age 26 ± 3 years, 22–33 y.o.); none presented any psychiatric symptoms. All were Caucasians, had education level equal or higher than high school corresponding to a mean of 14.9 ± 1.7 years of education, 70% of them were students, while 30% worked full time, and one of them was mother of a child.

3.2 | Radiosynthesis

Sterile [^{11}C]cetrozole ready for injection was produced with a radioactivity yield of 1.0 ± 0.6 GBq (n = 40), typically starting from 25 GBq [^{11}C]methyl iodide. The molar activity was 100 ± 60 GBq/μmol and the radiochemical purity was 98.5 ± 1%. The palladium concentration in the product solution was 8.4 ± 0.6 ng/ ml.

3.3 | Blood sampling and metabolite analysis

Figure 1 shows a typical whole blood activity curve from one subject as well as the mean plasma-to-whole blood ratio and mean fraction of intact tracer in the eight subjects with arterial blood samples. The mean plasma-to-whole blood ratio increased from 1.3 to 1.6 during the course of the scans and, on average, 26.6% of unmetabolized tracer was left in plasma at 90 min postinjection.

3.4 | Tracer kinetic analysis

Invasive kinetic models were evaluated: 1TCM, 2TCM, and plasma-input Logan. Typical TACs for the cerebellum, thalamus, and amygdala, from one representative subject, with the fits of 1TCM and 2TCM are given in Figure 2a–c. As expected, since the cerebellum has no or very low aromatase expression, both 1TCM and 2TCM were able to fit the cerebellum TAC. The 2TCM was able to fit the data well and was also preferred over 1TCM according the Akaike criteria for all TACs, except one TAC in one subject. However, it was not possible to robustly determine BP_{ND} directly from the 2TCM

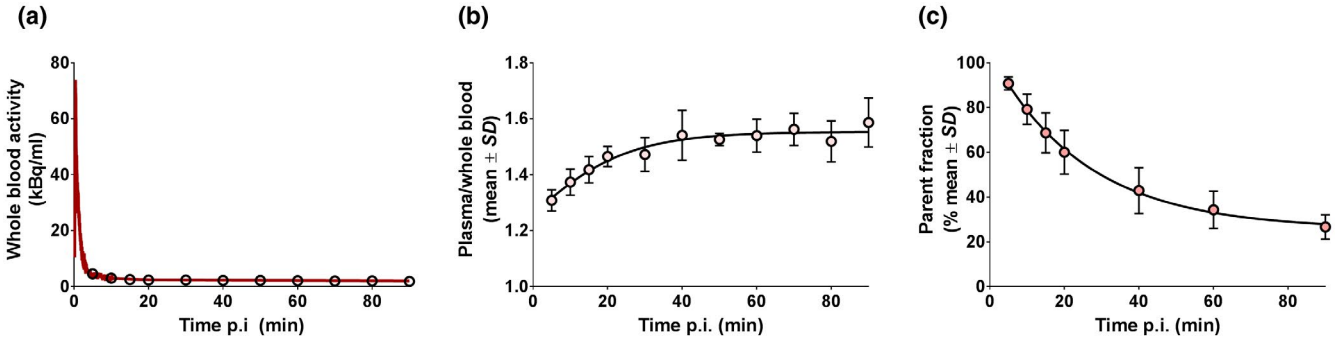

FIGURE 1 (a) A typical whole blood time–activity curve from one subject, (b) plasma-to-whole blood ratio, and (c) fraction of unmetabolized [^{11}C]cetrozole. Figures b and c present the mean ± *SD* of the eight participants with arterial blood sampling while the lines indicate sigmoid fits [Color figure can be viewed at wileyonlinelibrary.com]

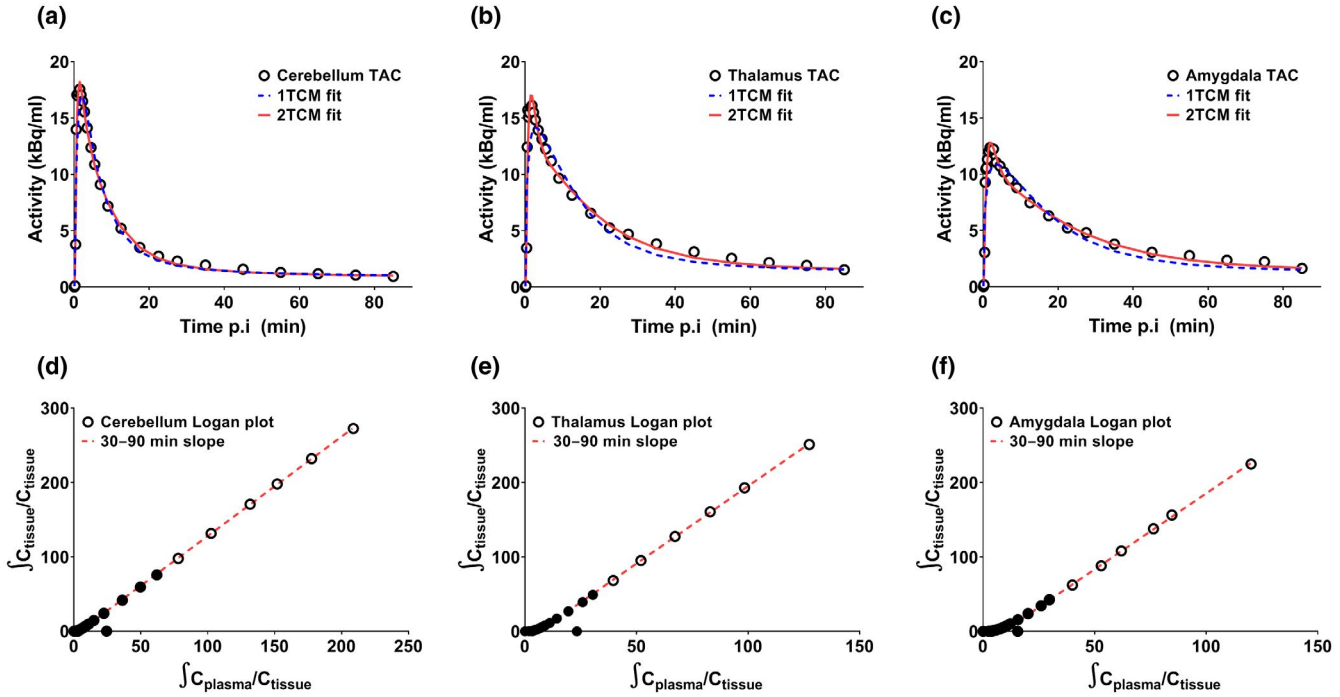

FIGURE 2 Compartment model fits and plasma-input Logan plots. Typical time–activity curves from one subject in the (a) cerebellum, (b) thalamus, and (c) amygdala, with fits of single-tissue (1TCM) and two-tissue (2TCM) reversible compartment models and plasma-input Logan plots from (d) cerebellum, (e) thalamus, and (f) amygdala, where the dotted line represent the slope of the time interval of 30–90 min [Color figure can be viewed at wileyonlinelibrary.com]

TABLE 1 Regional kinetic parameters from the 1TCM and 2TCM analysis. Values are the mean for each region with the range of the parameter in parentheses

	1TCM			2TCM					
Region	K_1	V_T	AIC	K_1	k_2	k_3	k_4	V_T	AIC
Thalamus	0.26 (0.20–0.30)	1.76 (1.39–2.18)	−20.39	0.45 (0.33–0.66)	0.86 (0.34–1.50)	0.42 (0.09–1.00)	0.19 (0.10–0.27)	1.78 (1.40–2.16)	−51.96
Amygdala	0.18 (0.14–0.21)	1.71 (1.44–2.00)	−30.30	0.26 (0.18–0.41)	0.40 (0.12–1.03)	0.22 (0.01–0.58)	0.13 (0.05–0.19)	1.78 (1.46–2.11)	−53.63
Hypothalamus	0.18 (0.15–0.23)	1.61 (1.20–1.86)	−33.22	0.27 (0.21–0.47)	0.60 (0.16–1.50)	0.39 (0.04–1.00)	0.17 (0.07–0.34)	1.66 (1.30–1.98)	−48.21
Putamen	0.32 (0.26–0.37)	1.38 (1.15–1.57)	−35.84	0.51 (0.36–0.68)	1.06 (0.31–1.50)	0.62 (0.04–1.00)	0.33 (0.09–0.45)	1.39 (1.17–1.60)	−63.63
Raphe	0.27 (0.21–0.34)	1.39 (1.12–1.68)	−31.63	0.39 (0.24–0.59)	0.74 (0.23–1.50)	0.52 (0.02–1.00)	0.55 (0.06–2.61)	1.43 (1.13–1.86)	−45.32
Cerebellum	0.34 (0.26–0.40)	1.23 (1.04–1.38)	−35.76	0.55 (0.41–0.72)	1.25 (0.39–1.50)	0.74 (0.05–1.00)	0.41 (0.18–0.64)	1.23 (1.04–1.36)	−53.52

as the standard errors frequently exceeded 25% of the BP_{ND} value itself. The kinetic parameters from 1TCM and 2TCM are given in Table 1, and as expected, the highest V_T was found in thalamus. Plasma-input Logan plots for cerebellum, thalamus, and amygdala in the same subject are shown in Figure 2d–f. The start time for the linear part of plasma-input Logan plots was decided from visual examination and was chosen to $t^* = 30$ min for all analyses. In Figure 2d–f, this time interval is represented by the open symbols in the graphs. The 1TCM DVR-1 values showed high correlation and agreement to the 2TCM DVR-1 values ($R^2 = 0.95$, slope = 0.90, confidence interval (CI) = 0.83–0.0.98) as given in Figure 3a. DVR-1 values from plasma-input Logan analyses were overestimated compared to the 2TCM DVR-1 values ($R^2 = 0.84$, slope = 1.20, CI = 1.02–1.37), while the V_T values from the two models showed a better agreement ($R^2 = 0.93$, slope = 1.06, CI = 0.96–1.16; Figure 3b,c). Slope values from the orthogonal regression analysis and the bias with the 95% limit of agreement between the methods are given in Table 2.

A mean 1TCM k_2-value in the cerebellum was calculated to 0.28 ± 0.015 and was used as the efflux constant in the LRTM DVR-1 calculations. However, omission of the k_2 term did not significantly change the DVR-1 values ($R^2 = 1.00$; slope = 1.00, CI = 0.99–1.01) and for the remainder of the study, only LRTM DVR-1 values without the k_2 term are reported.

In Figure 4, the relationships between 2TCM DVR-1 and the reference models are illustrated and corresponding slope, bias, and 95% limit of agreement are given in Table 2. An overall high correlation was seen between the plasma model and both LRTM and SRTM ($R^2 \geq 0.85$). LRTM DVR-1 values were overestimated (slope = 1.19, CI = 1.03–1.36), while SRTM BP_{ND} values were not (slope 1.01, CI = 0.89–1.14). SUVR-1 values showed a poorer correlation and were overestimated compared to 2TCM DVR-1. Multilinear regression did not show a significant effect of challenge on the relationship between SRTM BP_{ND} and 2TCM DVR-1.

3.5 | Parametric images

Parametric images from one subject (Figure 5) are provided, showing BP_{ND} calculated with RPM and RPM2 and DVR-1 calculated with LRTM on a time interval of 30–90 min. RPM and LRTM provided visually very similar parametric images while RPM2 gave a higher BP_{ND} in white matter areas. The relationship between VOI-based SRTM BP_{ND} and BP_{ND} and DVR-1 values extracted from the parametric images is given in Table 3, with the slopes of the orthogonal regression and R^2 values. In Table 3 is also slope and R^2 values given between SUVR-1 values and SRTM. All three parametric methods correlated well with VOI-based analysis of SRTM BP_{ND} ($R^2 \geq 0.90$). Agreement was good for RPM and LRTM with a slight overestimation compared to SRTM BP_{ND} (slope = 1.07 and 1.08) but with a very high correlation ($R^2 \geq 0.99$). Although RPM2 BP_{ND} also showed a high correlation with the VOI-based analysis, it was overestimated compared to SRTM BP_{ND} ($R^2 = 0.90$; slope = 1.48). The SUVR-1 values were also overestimated compared to SRTM BP_{ND} and had a lower correlation than the other

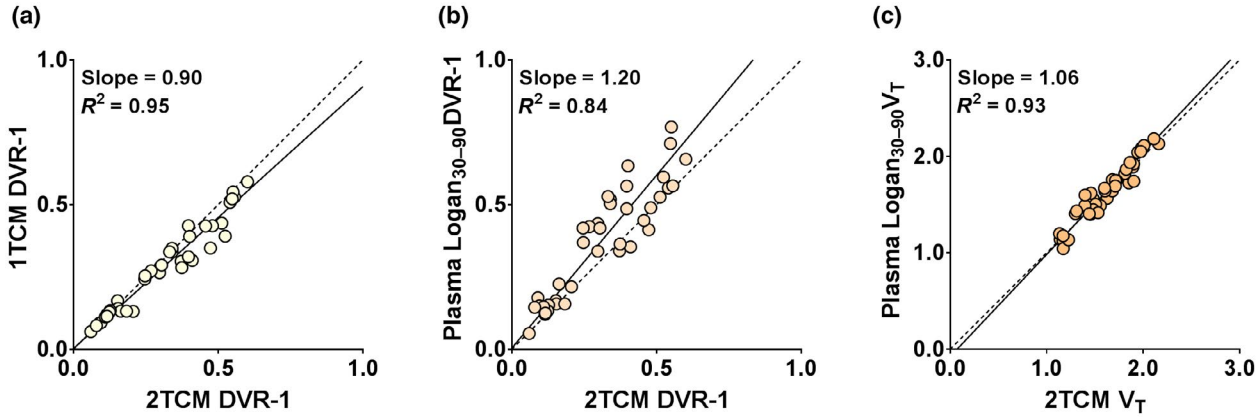

FIGURE 3 Correlations for plasma-input models. Relationship between DVR-1 of 2TCM and (a) 1TCM and (b) plasma-input Logan and (c) between V_T of 2TCM and plasma-input Logan. The solid lines represent the slope of the curve and the dotted lines are the lines of identity. *p* value for all correlation was <0.0001 [Color figure can be viewed at wileyonlinelibrary.com]

TABLE 2 Bias between the different methods together with the limits of agreement (LoA) and the slope of orthogonal regression with the confidence intervals (CI)

Methods	Bias (LoA)	Slope (CI)
1TCM DVR-1 versus 2TCM DVR-1	−0.02 (−0.10–0.05)	0.90 (0.83–0.97)
Plasma Logan DVR-1 versus 2TCM DVR-1	0.06 (−0.09–0.22)	1.20 (1.02–1.37)
Plasma Logan V_T versus 2TCM V_T	0.02 (−0.14–0.18)	1.06 (0.96–1.16)
LRTM DVR-1 versus 2TCM DVR-1	0.06 (−0.08–0.21)	1.19 (1.03–1.36)
SRTM BP_{ND} versus 2TCM DVR-1	0.01 (−0.10–0.13)	1.01 (0.89–1.14)
SUVR-1 versus 2TCM DVR-1	0.29 (−0.26–0.84)	2.85 (2.08–3.62)
LRTM DVR-1 versus Plasma Logan DVR-1	0.001 (−0.01–0.01)	1.00 (0.99–1.01)
SRTM BP_{ND} versus Plasma Logan DVR-1	−0.05 (−0.14–0.04)	0.86 (0.80–0.91)
SUVR-1 versus Plasma Logan DVR-1	0.22 (−0.25–0.7)	2.20 (1.77–2.64)

models. As expected, independent of the model, higher binding was observed in the thalamus and moderate levels in the amygdala.

3.6 | Scan duration

Two shortened scan durations of 60 and 40 min were analyzed in addition to the full 90-min data set, for all subjects. The relationship between the 90 min-based SRTM BP_{ND} and LRTM DVR-1 and the 60 and 40 min BP_{ND}, DVR-1, and SUVR-1 values are given in Figure 6, with the related slopes and correlations in the figure. SRTM BP_{ND} values were not notably affected by the decreased scan durations (slope = 0.98, CI = 0.977–0.984 and 0.93–1.04), except for the 40-min analysis of the putamen in one subject in two of the scans where the BP_{ND} values were highly overestimated compared to the 90-min SRTM BP_{ND} values (Figure 6b). LRTM DVR-1 on a time interval of 30–60 and 20–40 min both showed a high correlation to the 30–90 min DVR-1 (R^2 = 0.98 and 0.97, respectively), while the 60-min data set was in good agreement (slope = 0.95, CI = 0.93–0.97) and the 40-min data set was underestimated compared to the 30- to 90-min analysis (slope = 0.80, CI = 0.77–0.82). SUVR-1 showed a higher correlation to both SRTM and LRTM DVR-1 for the 40- and 60-min data sets compared to the full scan duration (R^2 = 0.91–0.93) but was still highly overestimated (slope = 1.58–2.15). In all graphs in Figure 6 there are three points with a value around 1.5. These points correspond to the thalamus region, in the three different scans, of one subject. *p* value for all correlations was <0.0001.

3.7 | Simulations

Absolute (relative) accuracy and precision of 2TCM DVR-1 ranged from 0.00 (−0.6%) (bias) and 0.02 (5.9%) (COV) for rate constants corresponding to thalamus, 0.00 (−0.2%) and 0.02 (6.0%) for amygdala, to 0.00 (−8.4%) and 0.01 (140%) for raphe. For SRTM BP_{ND}, these values were 0.00 (−0.9%) and 0.05 (14.2%), 0.01 (2.3%) and 0.02 (6.8%), and −0.02 (−209%) and 0.04 (363%), respectively.

4 | DISCUSSION

In the present study, tracer kinetics for quantitation of the novel aromatase PET tracer [^{11}C]cetrozole were evaluated, using both plasma-input as well as reference tissue models. Different methods

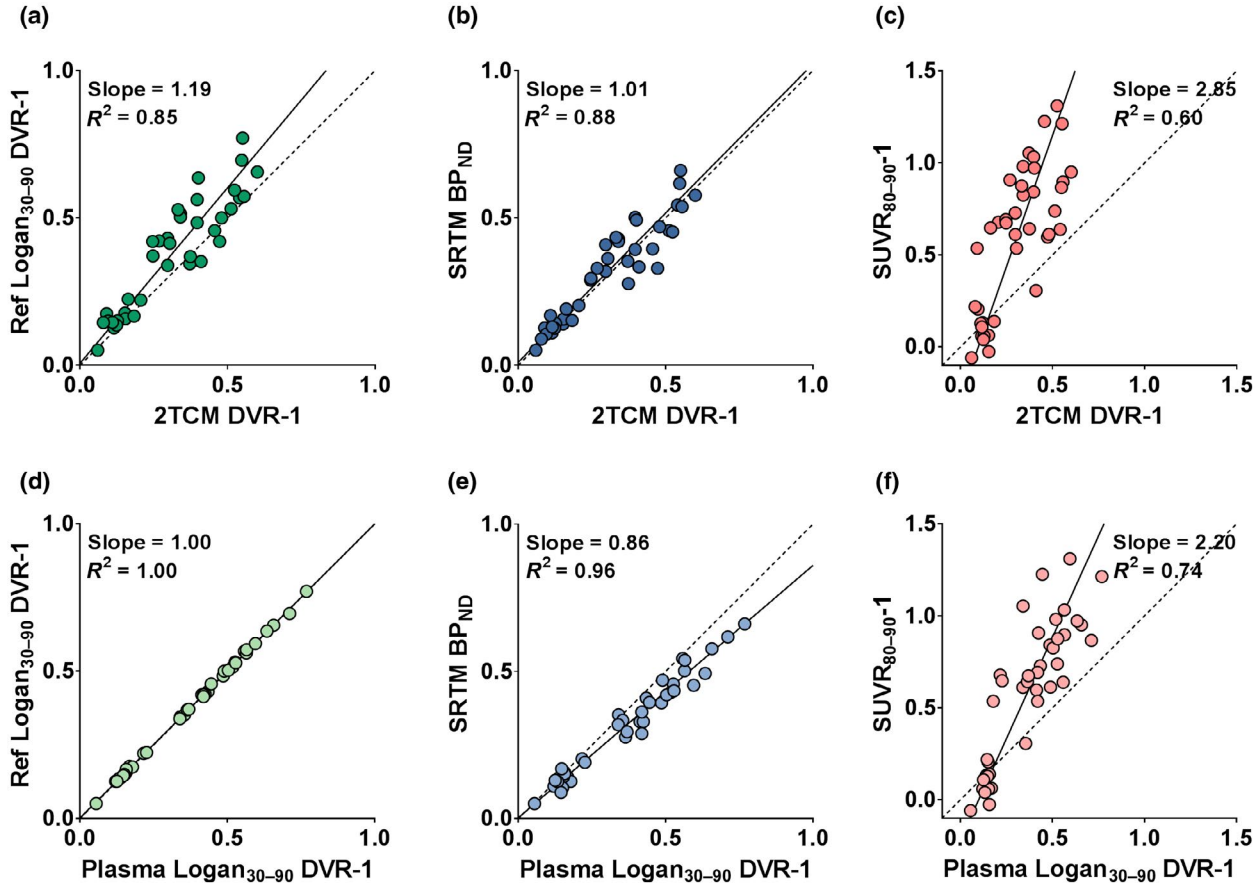

FIGURE 4 Correlations for the reference tissue models. Relationship between 2TCM DVR-1 and (a) LRTM DVR-1, (b) SRTM BP_{ND}, and (c) SUVR-1 and between plasma-input Logan DVR-1 and (d) LRTM DVR-1, (e) SRTM BP_{ND}, and (f) SUVR-1. The solid lines represent the slope of the curve and the dotted lines are the lines of identity. *p* value for all correlation was <0.0001 [Color figure can be viewed at wileyonlinelibrary.com]

TABLE 3 Square of Pearson's correlation coefficient (R^2) and slope of orthogonal regression with the confidence intervals (CI) of the parametric methods relative to VOI-based SRTM BP_{ND}

Voxel-wise analysis	VOI-based analysis	
	SRTM BP_{ND}	
Parametric methods	R^2	Slope (CI)
RPM BP_{ND}	0.99	1.07 (1.06–1.08)
RPM2 BP_{ND}	0.90	1.48 (1.40–1.55)
LRTM DVR-1	0.99	1.08 (1.06–1.10)
SUVR$_{80-90}$-1	0.85	2.30 (2.15–2.45)

Note: *p* value for all correlation was <0.0001.

to generate parametric images of [^{11}C]cetrozole binding have also been tested, as well as shortened PET scan duration. Reference tissue models showed a high correlation and agreement with plasma-input models, and a scan duration of 60 min was sufficient to obtain robust binding estimates. Further, as demonstrated in nonhuman primates (Takahashi et al., 2014), the cerebellum can be used as reference region.

To identify the optimal model to describe the *in vivo* kinetics of [^{11}C]cetrozole PET, VOI-based analysis was performed using single-tissue and two-tissue reversible plasma-input compartment models and Logan graphical analyses (Akaike, 1974; Logan et al., 1990). Additionally, simplified reference tissue model (Lammertsma & Hume, 1996), and Logan reference tissue model, analyses (Logan et al., 1996) were performed with cerebellum as reference region, as done by (Takahashi et al., 2014). The [^{11}C]cetrozole TACs were best described by the 2TCM, according to the AIC, compared to 1TCM. DVR-1 values from plasma-input Logan analyses were overestimated compared to the 2TCM DVR-1 values, while the V_T values from the two models were in better agreement. Both SRTM and LRTM agreed well with the plasma-input binding results, but the highest agreement was observed between SRTM BP_{ND} values and 2TCM DVR-1. We did not correct for clearance from the reference tissue in the LRTM analyses, as omission of the k_2 term did not change the DVR-1 values. Further, substantiating this choice, we found excellent agreement between the plasma-input Logan and LRTM DVR-1 values. Reference tissue models correlated well with plasma-input models, thus indicating that arterial blood sampling is not necessary. This is in line with the results in nonhuman primates showing a strong correlation between arterial blood sampling as the input function (Vt)

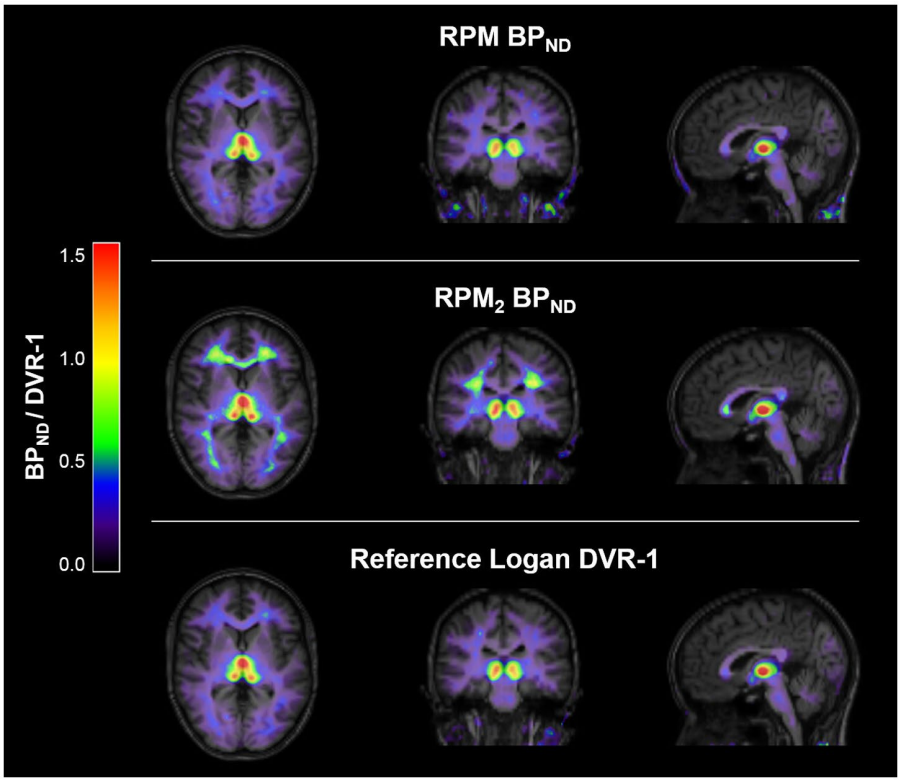

FIGURE 5 Parametric images of (a) RPM BP_{ND}, (b) RPM_2 BP_{ND}, and (c) LRTM DVR-1 from one subject. Images are fused over the co-registered MRI of the subject [Color figure can be viewed at wileyonlinelibrary.com]

and Logan reference tissue model based on the average k_2' (BP_{ND}) (Takahashi et al., 2014). Simulations showed that 2TCM DVR-1 and SRTM BP_{ND} can be estimated with a high accuracy and precision in high-binding regions such as thalamus and amygdala. Accuracy and precision in absolute terms are comparable in low-binding regions such as the raphe, but relative accuracy and precision are poor due to the very low absolute values of DVR-1 and BP_{ND} in these regions.

Additionally, as a semi-quantitative measure, SUVR was analyzed to evaluate potential simplification of the data acquisition. SUVR overestimated the binding compared to both the plasma-input and the reference tissue models on an 80–90 min interval. Although SUVR-1 values were reduced for the earlier intervals of 30–40 and 50–60 min, they still resulted in overestimations of about 50%–100% compared to SRTM BP_{ND} and LRTM DVR-1. In addition, correlation was moderate at best ($R^2 = 0.6$), making a single time point scan not a suitable option for quantification of [^{11}C]cetrozole binding.

To validate the voxel-level analyses, parametric images were compared with VOI-based analyses. RPM BP_{ND} and LRTM DVR-1 values, extracted from the parametric images, agreed well with VOI-based SRTM BP_{ND} values. RPM and LRTM also produced visually very similar images of the aromatase binding. RPM2 BP_{ND} yielded higher values in white matter areas, and the extracted BP_{ND} values were overestimated compared to the VOI-based reference methods. This may be due to an incorrect determination of the efflux rate constant, estimated from the previous RPM calculation and fixed for the RPM2 analysis. However, no optimization of the determination of this constant, for example by only using k_2' values from pixels with a higher cutoff value for BP_{ND}, was performed since both RPM and LRTM provided quantitatively accurate binding images.

Neither SRTM BP_{ND} nor LRTM DVR-1 values were notably affected when we shortened the scan duration to 60 min. However, when further decreasing the scan duration to 40 min, LRTM underestimated DVR-1 values for the 20–40 min interval compared to the 30–90 min interval. The 40-min SRTM BP_{ND} values still showed a high agreement compared to the 90-min BP_{ND} values, while there was a slight decrease in correlation due to two outliers for one subject where 40-min data did not give a good fit. This suggests that a 60-min scan duration, as previously applied by Takahashi et al. (2018), but not shorter, is sufficient for the quantification of [^{11}C]cetrozole binding, thus reducing patient burden.

A strength of the present study is the assessment of quantitative measurements obtained through kinetic modeling of the PET data, including plasma- and reference tissue-based methods, as previously done in nonhuman primates (Takahashi et al., 2014). Moreover, to evaluate [^{11}C]cetrozole binding with plasma-input-based kinetic analysis, a metabolite-corrected arterial input function was employed. In contrast, the PET examinations in this study were performed on three different PET scanners with varied reconstruction settings. Although different scanners and reconstruction parameters may affect the results of the quantification of the PET data, the reconstructions for scans from different scanners were chosen to match each other in terms of spatial resolution. Any remaining differences between the scanners will likely not affect the conclusions

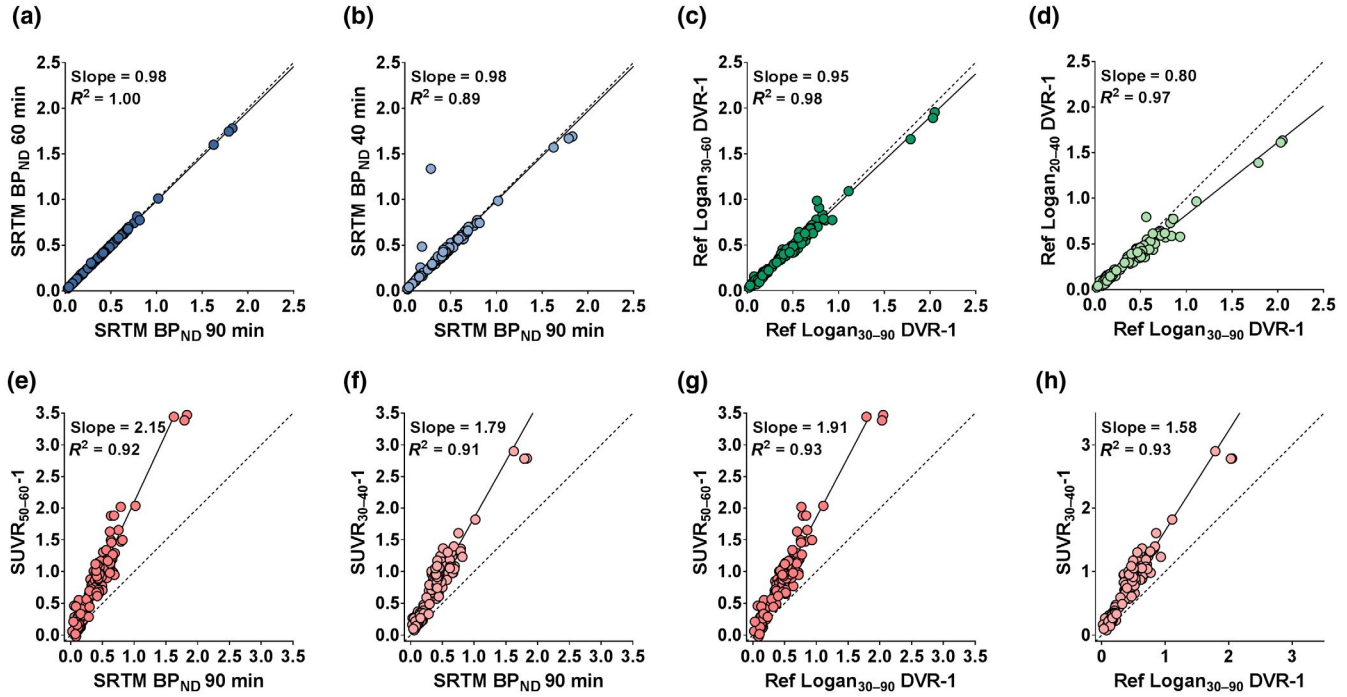

FIGURE 6 Relationship between SRTM BP_{ND} of the full 90-min scan and (a) 60-min SRTM BP_{ND}, (b) 40-min SRTM BP_{ND}, (e) 50-60 min SUVR-1 and (f) 30-40 min SUVR-1 and between LRTM DVR-1 on a time interval of 30–90 min and (c) LRTM DVR-1 of 30–60 min, (d) LRTM DVR-1 of 20–40 min, (g) 50-60 min SUVR-1 and (h) 30-40 min SUVR-1. The solid lines represent the slope of the curve and the dotted lines are the lines of identity. *p* value for all correlation was <0.0001 [Color figure can be viewed at wileyonlinelibrary.com]

of the present work since the different methods for quantifying the binding only were compared within scans. Currently, [^{11}C]cetrozole is the sole and best available tracer for aromatase. To our knowledge, this is the first study systematically assessing tracer kinetics of [^{11}C]cetrozole, including arterial plasma data, in healthy women. The present results are expected to apply also to men, as sex is not expected to influence the outcome parameters of the present study. The investigated VOIs (i.e., thalamus, hypothalamus, putamen, raphe nuclei, and amygdala) are putative brain regions of interest to behavior and mental health. A validated, quantitative PET measure for [^{11}C]cetrozole is therefore useful to investigate testosterone–estrogens dynamics in the healthy brain (Takahashi et al., 2014), as well as how these are influenced by pathophysiological conditions or pharmacological treatments.

5 | CONCLUSION

SRTM using cerebellum as reference region appears to be the optimal method to noninvasively estimate [^{11}C]cetrozole binding. SRTM BP_{ND} values were highly correlated with the plasma-input models, with the highest agreement between SRTM BP_{ND} and 2TCM DVR-1. To generate parametric images of the [^{11}C]cetrozole binding, the basis function implementation of SRTM, RPM, and the LRTM method were equivalent, with high agreement to the VOI-based reference methods and visually very similar images. SRTM generated robust and quantitatively accurate results for a shortened scan, suggesting that 60-min scan duration is sufficient for accurate quantification of [^{11}C]cetrozole PET. In summary, [^{11}C]cetrozole can be employed as PET tracer for relatively short-dynamic brain scans and reference tissue-based analyses to image aromatase in the human brain.

ACKNOWLEDGMENTS

We thank the research nurses Kaisa Lyon and Mimmi Lidholm and the staff at the PET center and Lena Moby at the KBH unit; Julia Breedh, Haro de Grauw, Adine Yeganeh, Lieve Visscher, Gianvito Lagravinese, Maria Helou, Anna Persson, and Axel Mohss, students who helped with the BSH study; and Dr. Jean Pettersson, Uppsala University for quantification of palladium by ICP-AES.

CONFLICT OF INTEREST

No conflicting interests exist.

AUTHOR CONTRIBUTIONS

All the authors had full access to all the data in the study and take responsibility for the integrity of the data and the accuracy of the data analysis. *Conceptualization*, E.C., I.S.P., K.T., G.A., Y.W., and M.L.; *Methodology*, M.L., M.J., K.T., T.N., and T.H.; *Software*, M.L. and M.J.; *Investigation*, E.C., I.S.P., G.A., and J.W.; *Formal Analysis*, M.J., P.N., H.W., J.E., M.L., and E.C.; *Resources*, K.T., Y.W., E.C., I.S.P., G.A., and J.W.; *Data Curation*, M.J., M.L., E.C., and I.S.P.; *Writing – Original Draft*, M.J., E.C., M.L.; *Writing – Review & Editing*, E.C., M.J., M.L., K.T., Y.W., G.A., J.W., and J.E.; *Visualization*, M.J. and M.L.; *Supervision*, E.C., M.L., G.A., and J.W.; *Project Administration*, K.T., Y.W., E.C., I.S.P., G.A., and J.W.; *Funding Acquisition*, I.S.P.

PEER REVIEW

The peer review history for this article is available at https://publons.com/publon/10.1002/jnr.24707.

DATA AVAILABILITY STATEMENT

Due to the nature of the present study, participants of this study did not agree for their data to be shared publicly, so supporting data are not available.

ORCID

Jonas Eriksson https://orcid.org/0000-0003-0241-092X
Inger Sundström Poromaa https://orcid.org/0000-0002-2491-2042
Mark Lubberink https://orcid.org/0000-0001-8324-7399
Erika Comasco https://orcid.org/0000-0002-2174-2068

REFERENCES

Akaike, H. (1974). A new look at the statistical model identification. *IEEE Transactions on Automatic Control*, *19*(6), 716–723. https://doi.org/10.1109/TAC.1974.1100705

Biegon, A. (2015). In vivo visualization of aromatase in animals and humans. *Frontiers in Neuroendocrinology*, *40*, 42–51. https://doi.org/10.1016/j.yfrne.2015.10.001

Biegon, A., Alexoff, D. L., Kim, S. W., Logan, J., Pareto, D., Schlyer, D., … Fowler, J. S. (2015). Aromatase imaging with [N-methyl-11C]vorozole PET in healthy men and women. *Journal of Nuclear Medicine*, *56*(4), 580–585. https://doi.org/10.2967/jnumed.114.150383

Biegon, A., Kim, S. W., Alexoff, D. L., Jayne, M., Carter, P., Hubbard, B., … Fowler, J. S. (2010). Unique distribution of aromatase in the human brain: In vivo studies with PET and [N-methyl-11C]vorozole. *Synapse*, *64*(11), 801–807. https://doi.org/10.1002/syn.20791

Brocca, M. E., & Garcia-Segura, L. M. (2019). Non-reproductive functions of aromatase in the central nervous system under physiological and pathological conditions. *Cellular and Molecular Neurobiology*, *39*(4), 473–481. https://doi.org/10.1007/s10571-018-0607-4

Gunn, R. N., Gunn, S. R., & Cunningham, V. J. (2001). Positron emission tomography compartmental models. *Journal of Cerebral Blood Flow and Metabolism*, *21*(6), 635–652. https://doi.org/10.1097/00004647-200106000-00002

Gunn, R. N., Lammertsma, A. A., Hume, S. P., & Cunningham, V. J. (1997). Parametric imaging of ligand-receptor binding in PET using a simplified reference region model. *NeuroImage*, *6*(4), 279–287. https://doi.org/10.1006/nimg.1997.0303

Ishunina, T. A., van Beurden, D., van der Meulen, G., Unmehopa, U. A., Hol, E. M., Huitinga, I., & Swaab, D. F. (2005). Diminished aromatase immunoreactivity in the hypothalamus, but not in the basal forebrain nuclei in Alzheimer's disease. *Neurobiology of Aging*, *26*(2), 173–194. https://doi.org/10.1016/j.neurobiolaging.2004.03.010

Lammertsma, A. A., & Hume, S. P. (1996). Simplified reference tissue model for PET receptor studies. *NeuroImage*, *4*(3 Pt 1), 153–158. https://doi.org/10.1006/nimg.1996.0066

Logan, J., Fowler, J. S., Volkow, N. D., Wang, G. J., Ding, Y. S., & Alexoff, D. L. (1996). Distribution volume ratios without blood sampling from graphical analysis of PET data. *Journal of Cerebral Blood Flow and Metabolism*, *16*(5), 834–840. https://doi.org/10.1097/00004647-199609000-00008

Logan, J., Fowler, J. S., Volkow, N. D., Wolf, A. P., Dewey, S. L., Schlyer, D. J., … Gatley, S. J. (1990). Graphical analysis of reversible radioligand binding from time-activity measurements applied to [N-11C-methyl]-(-)-cocaine PET studies in human subjects. *Journal of Cerebral Blood Flow and Metabolism*, *10*(5), 740–747. https://doi.org/10.1038/jcbfm.1990.127

Sasano, H., Takashashi, K., Satoh, F., Nagura, H., & Harada, N. (1998). Aromatase in the human central nervous system. *Clinical Endocrinology*, *48*(3), 325–329. https://doi.org/10.1046/j.1365-2265.1998.00390.x

Sheehan, D. V., Lecrubier, Y., Sheehan, K. H., Amorim, P., Janavs, J., Weiller, E., … Dunbar, G. C. (1998). The Mini-International Neuropsychiatric Interview (M.I.N.I.): The development and validation of a structured diagnostic psychiatric interview for DSM-IV and ICD-10. *Journal of Clinical Psychiatry*, *59*(Suppl. 3), 22–33; quiz 34–57.

Svarer, C., Madsen, K., Hasselbalch, S. G., Pinborg, L. H., Haugbøl, S., Frøkjær, V. G., … Knudsen, G. M. (2005). MR-based automatic delineation of volumes of interest in human brain PET images using probability maps. *NeuroImage*, *24*(4), 969–979. https://doi.org/10.1016/j.neuroimage.2004.10.017

Takahashi, K., Hosoya, T., Onoe, K., Doi, H., Nagata, H., Hiramatsu, T., … Watanabe, Y. (2014). 11C-cetrozole: An improved C-11C-methylated PET probe for aromatase imaging in the brain. *Journal of Nuclear Medicine*, *55*(5), 852–857. https://doi.org/10.2967/jnumed.113.131474

Takahashi, K., Hosoya, T., Onoe, K., Takashima, T., Tanaka, M., Ishii, A., … Watanabe, Y. (2018). Association between aromatase in human brains and personality traits. *Scientific Reports*, *8*(1), 16841. https://doi.org/10.1038/s41598-018-35065-4

Thomas, M. P., & Potter, B. V. (2013). The structural biology of oestrogen metabolism. *Journal of Steroid Biochemistry and Molecular Biology*, *137*, 27–49. https://doi.org/10.1016/j.jsbmb.2012.12.014

Wu, J.-L., He, Y., Hrubý, R., Balesar, R., Qi, Y.-J., Guo, L., … Bao, A.-M. (2017). Aromatase changes in depression: A postmortem and animal experimental study. *Psychoneuroendocrinology*, *77*, 56–62. https://doi.org/10.1016/j.psyneuen.2016.11.026

Wu, Y., & Carson, R. E. (2002). Noise reduction in the simplified reference tissue model for neuroreceptor functional imaging. *Journal of Cerebral Blood Flow and Metabolism*, *22*(12), 1440–1452. https://doi.org/10.1097/00004647-200212000-00004

SUPPORTING INFORMATION

Additional supporting information may be found online in the Supporting Information section.

Transparent Peer Review Report

How to cite this article: Jonasson M, Nordeman P, Eriksson J, et al. Quantification of aromatase binding in the female human brain using [^{11}C]cetrozole positron emission tomography. *J Neurosci Res*. 2020;98:2208–2218. https://doi.org/10.1002/jnr.24707